

# Formulation and Evaluation of a Silymarin Inclusion Complex-Based Gel for Skin Cancer

Wael A. Mahdi, Syed Sarim Imam,\* Abdulkarim Alotaibi, Saad Alhallaf, Riyad F. Alzhrani, and Sultan Alshehri\*

Cite This: *ACS Omega* 2025, 10, 3006–3017

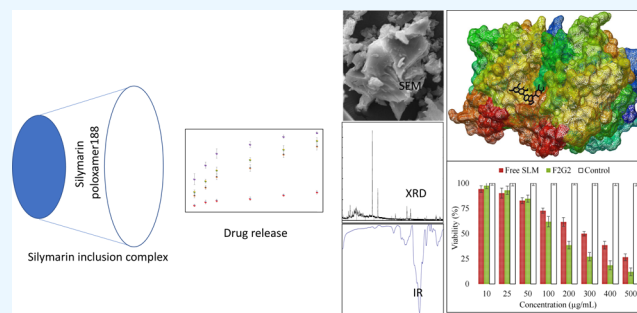
Read Online

ACCESS |

Metrics & More

Article Recommendations

**ABSTRACT:** Silymarin (SLM) is a bioactive, water-insoluble flavonoid reported against different types of cancer. In the present research, the SLM inclusion complex was prepared by the freeze-drying method using different cyclodextrins. The phase solubility study was performed to assess the stability constant and complexation efficiency. The prepared SLM inclusion complexes (F1, F2, and F3) were characterized for different physicochemical and in vitro parameters. Based on the results, the selected inclusion complex (F2) was converted to a topical gel. Finally, it was evaluated for antioxidant, protein denaturation, and cell viability assay (B16F10; skin cancer cell line). The in vitro results were further confirmed by performing a molecular docking study. The phase solubilization results showed the formation of a stable complex with a stability constant value of  $548 \text{ mol L}^{-1}$  ( $\beta\text{CD-PLX}$ ),  $911 \text{ mol L}^{-1}$  (HP  $\beta\text{CD-PLX}$ ), and  $736 \text{ mol L}^{-1}$  (M  $\beta\text{CD-PLX}$ ). A marked increase in release pattern was found from the prepared inclusion complex ( $80.9 \pm 2.2$ – $97.8 \pm 3.1\%$ ) compared to free SLM ( $24.1 \pm 2.8\%$ ). DSC as well as the IR studies confirm the formation of a stable complex. SEM and X-ray diffraction results confirmed the conversion to the amorphous form. The molecular docking studies exhibited the high docking score of SLM with both colchicine-binding sites of the tubulin protein ( $-6.28 \text{ kcal/mol}$ ) and complexing agents, viz.,  $\beta\text{CD}$  ( $-4.61 \text{ kcal/mol}$ ), HP  $\beta\text{CD}$  ( $-5.77 \text{ kcal/mol}$ ), and M  $\beta\text{CD}$  ( $-5.61 \text{ kcal/mol}$ ). The antioxidant assay results showed that the activity was significantly improved (1.2–1.6 fold) compared to free SLM. The in vitro cell viability assay outcome displayed concentration-dependent activity with a significantly lower IC<sub>50</sub> value from F2G2 ( $145.3 \pm 4.2 \mu\text{g/mL}$ ) than free SLM ( $304.7 \pm 5.7 \mu\text{g/mL}$ ). The above conclusions demonstrated that the developed SLM inclusion complex-based gel system could be an ideal delivery system for skin cancer.



## INTRODUCTION

Silymarin (SLM; [Figure 1](#)) is a flavonoid obtained from milk thistle seed extract and has drawn much interest in the treatment of a variety of illnesses.<sup>1–3</sup> The primary and most active component of SLM is silibinin, which constitutes about 60–70% of flavonoids. Other active ingredients include

isosilybinin, silydianin, and silychristin.<sup>4,5</sup> Its antioxidant, anti-inflammatory, and immunomodulatory properties are responsible for SLM therapeutic action in various diseases. Recent preclinical and clinical research has reported that SLM has shown therapeutic effects in wound healing, vitiligo, psoriasis, melanoma, UV-induced erythema, and nonmelanoma skin cancer.<sup>6,7</sup> In the tubulin-colchicine receptor (protein), the colchicine binding site always remains the favored target for the evolution of novel drugs to manage human ill-health including cancer.<sup>8</sup> The microtubules were found to be effective targets for different antimetabolic agents. The past study indicates that the planar or biaryl configuration was a required feature

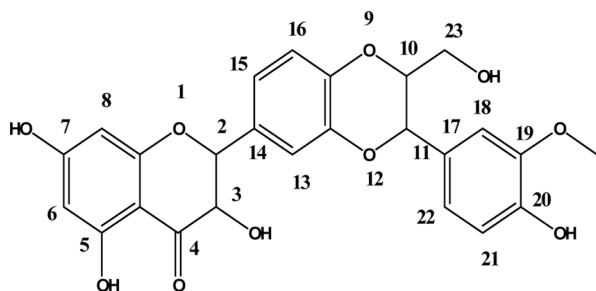
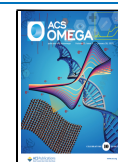
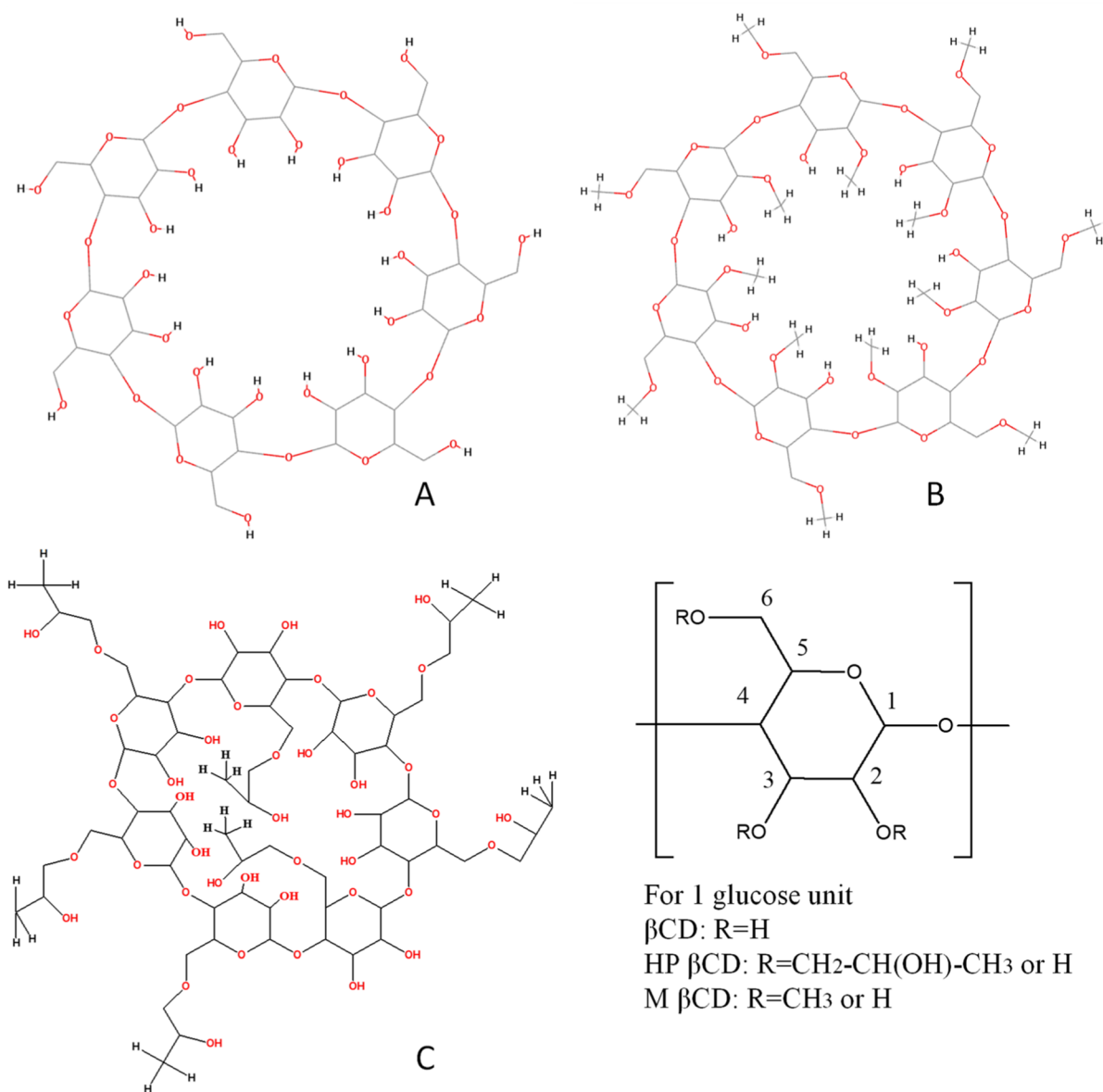


Figure 1. Chemical structure of SLM.

Received: October 22, 2024  
Revised: November 27, 2024  
Accepted: December 20, 2024  
Published: January 13, 2025





**Figure 2.** 2D schematic structure of (A) Beta CD, (B) methyl beta CD (software: BIOVIA Discovery Studio, 2024), and (C) hydroxy propyl beta CD (software: Chem3D 14.0 suite).

for the drug to interact at the colchicine binding site.<sup>9</sup> The low aqueous solubility and bioavailability limit its biological activity.<sup>3</sup> Therefore, to improve therapeutic efficacy, SLM solubility must be increased by preparing various formulations like the cyclodextrin (CD) inclusion complex,<sup>5,7,10–12</sup> phospholipid complex,<sup>13</sup> and solid dispersion.<sup>14</sup>

CD is a cyclic oligosaccharide that is produced when glucosyltransferase breaks down starch. It comprises six to 12 D-(+)-glucopyranose units arranged in a chair conformation and joined by  $\alpha$ -1,4-glucosidic linkages.<sup>15</sup> The most popular CDs—referred to as  $\alpha$ -CD,  $\beta$ -CD, and  $\gamma$ -CD—have 6, 7, and 8 glucose units. These CDs have a lipophilic core with a hydrophilic outer surface, which helps to form noncovalent inclusion complexes with insoluble drugs by being taken up partially or completely into the cavity.<sup>16</sup> In the modification with an alkyl moiety, like hydroxyalkyl or methyl, on free hydroxyl groups of  $\beta$ CD, the complexing ability of CD derivatives was significantly modified.<sup>12</sup>

$\beta$ CD (Figure 2A) is the most commonly utilized in the pharmaceutical industries. It has a medium cavity size and inexpensive production costs.<sup>17</sup> With their exclusive assembly of a hydrophilic exterior wall and a hydrophobic inner chamber, it can enclose a wide range of hydrophobic molecules that are of the right size and shape. These properties result in a high inclusion rate and improved molecular stability and solubility.<sup>18</sup> The solubility is significantly enhanced by the random substitution of the hydroxy groups.<sup>19</sup> HP $\beta$ CD and M  $\beta$ CD are examples of CD derivatives that are of pharmacological interest. Compared with  $\beta$ CD, M  $\beta$ CD (Figure 2B) exhibits an improved water solubility of up to 50 times. HP  $\beta$ CD (Figure 2C) has the highest aqueous solubility ( $\geq 600$  mg/mL) and is used in various pharmaceutical formulations.<sup>20,21</sup> The inner surface of the torus becomes more hydrophobic and has less steric hindrance due to the methylation of the CD ring, which might then increase the entrapment efficiency.<sup>22</sup>

The topical route is an alternative route of drug administration and has several potential benefits. These benefits include avoiding hepatic first-pass metabolism, site-specific drug delivery, prolonged duration of action, and reducing unwanted systemic side effects. When long-term or chronic medication therapy is needed, the topical route is especially noteworthy for its efficacy.<sup>23</sup> Generally, the usage of CDs has been shown to improve drug stability, tolerance, apparent solubility, and controlled release of drugs into the skin.<sup>24</sup> CDs are also perfect penetration enhancers because they can improve drug delivery via biological barriers without impairing their barrier function.<sup>25</sup>

The present study was designed to develop an SLM inclusion complex using different CDs with Poloxamer 188 (PLX) by the freeze-drying method. The addition of PLX to the inclusion complex may promote interactions between SLM and CDs, which can result in relevant alteration in the physicochemical properties of the supramolecular inclusion complex. The formed complex was evaluated for drug release and for other characterization parameters. Based on maximum drug release, the selected complex is further entrapped into the Carbopol 934 polymer to form a gel system to enhance the residence time on the skin. The optimized topical gel was characterized and further evaluated for antioxidant, protein denaturation, and cell viability study. The molecular docking was also performed to assess and support the findings of *in vitro* anticancer activity.

## MATERIALS AND METHODS

**Materials.** The different CDs like beta cyclodextrin ( $\beta$ CD, MW 1134.9, AR  $\geq$  98%), hydroxy propyl beta cyclodextrin (HP  $\beta$ CD, AR  $\geq$  98%, degree of substitution 4–9), and methyl beta cyclodextrin (M  $\beta$ CD, white powder, MW = 1190 and an average degree of substitution, DS = 0.5) were procured from Sigma-Aldrich, MO, USA. The pure SLM (yellow powder, MW 482.6, CAS number 65666-07-1) was purchased from Sigma-Aldrich, Switzerland. Poloxamer 188 was purchased from Alfa Aesar Ward Hill MA. A Standard DPPH kit (2,2-diphenyl-1-picryl hydrazine) and Albumin bovine were purchased from Spectro Chem Pvt. Ltd., Mumbai, India and UFC Biotechnology Amherst, NY, USA.

**Methods.** *Phase Solubility Study.* The study was performed to evaluate the different parameters like complexation efficiency and apparent 1:1 stability constant.<sup>26</sup> The different molar concentrations of aqueous  $\beta$ CD (0–16 mM), HP  $\beta$ CD, and M  $\beta$ CD solutions (0–50 mM) with a fixed concentration of PLX (5%, w/w) were prepared in double distilled water (25 mL). The solution was vortexed for complete solubilization, and then, an excess amount of SLM (ternary system) was transferred to the flask. The dispersions were kept on the orbital water shaker for 48 h with shaking at 37 °C. Two mL of the samples from each flask was collected, and the filtrate was diluted (if needed) to measure SLM concentration using UV spectroscopy (Shimadzu 1801 PC, Kyoto, Japan) at 286 nm. The absorbance was used to calculate SLM concentration and the different parameters were calculated using the following formula<sup>27</sup>

$$\text{stability constant (Ks 1: 1)} = \frac{\text{slope}}{\text{So}(1 - \text{slope})} \quad (1)$$

where So: free SLM intrinsic water solubility.

$$\text{complexation efficiency (CE)} = \frac{\text{slope}}{(1 - \text{slope})} \quad (2)$$

*Formulation of the Inclusion Complex.* The freeze-drying method was employed to formulate the SLM inclusion complex using different CDs ( $\beta$ CD-PLX; HP  $\beta$ CD-PLX; M  $\beta$ CD-PLX) as shown in Table 1. First, SLM was dissolved in

**Table 1. Composition of the SLM Inclusion Complex Using Different CDs<sup>a</sup>**

code	SLM	$\beta$ CD	HP $\beta$ CD	M $\beta$ CD	Poloxamer 188 (w/w)
F1	1	1			5%
F2	1		1		5%
F3	1			1	5%

<sup>a</sup>Drug and CDs taken in molar ratio.

alcohol, and separately CDs-PLX was dissolved in double distilled water. Both solutions were mixed slowly with stirring, and then the organic phase was evaporated by a rotary evaporator (HAHNVAPOR-2005S-N, HAHNSHIN, Korea). Finally, the remaining aqueous solution was lyophilized in a freeze-dryer (Alpha 1–2 LD Plus, Martin Christ, Germany). The lyophilization was done by prefreezing at –20 °C for 3 h and then pre-frozen at –80 °C for 6 h. The frozen samples were lyophilized at –50 °C for 24 h.<sup>28,29</sup> The freeze-dried product was collected and dried at 40 °C for 3 h and stored in a glass container for further use.

*Dissolution Study.* The drug release of free SLM and SLM inclusion complex (F1, F2, and F3) was studied using the dissolution instrument (DISTEK dissolution system). Each sample (~10 mg of SLM) was filled into empty gelatin capsules and dipped into the dissolution medium (900 mL). The study was performed for 1 h at a temperature of 37 °C with a rotation speed of 50 rpm. The released content was collected at a fixed time point and then replaced with fresh release medium. The samples were filtered and diluted (if needed) to estimate the SLM concentration using UV spectroscopy at 278 nm. The released data were fitted to different kinetic models to calculate the release mechanisms.

*Infrared Spectroscopy.* The drug carrier interaction study was assessed by the infrared spectroscopy method (ATR Bruker Alpha Germany). The free SLM, HP  $\beta$ CD, PLX, physical mixture, and inclusion complex (F2) were scanned (4000–400  $\text{cm}^{-1}$ ) and their characteristic functional group peaks were compared with each other to assess the changes in the chemical bonds and functional groups.

*Differential Scanning Calorimetry.* The free SLM and inclusion complex (F2) were scanned using a DSC instrument (Perkin Elmer, Shelton, USA) in the temperature range of 40–300 °C. It gives the thermal behavior of SLM after the formation of the inclusion complex. Each sample was sealed in an aluminum pan and scanned with a heating speed of 10 °C/min with a continuous flow of inert nitrogen.

*Scanning Electron Microscopy.* Scanning electron microscopy (ZEISS Cambridge UK) of the free SLM and inclusion complex (F2) was performed to observe the change in the surface morphology. It gives an idea of conversion to the amorphous form from the crystalline structure after the formation of the inclusion complex. The free SLM and F2 images were taken on a grid coated with gold before the images were taken.

**Table 2. Formulation and Characterization of SLM Inclusion Complex-Based Gels**

code	Carbopol 934P (% w/v)	PEG 200 (% w/v)	Chlorocresol (% w/v)	viscosity (cP)	spreadability (cm <sup>2</sup> )	drug content (%)
F2G1	0.8	10	1	1787 ± 22	7.4 ± 0.8	99.43 ± 3.4
F2G2	1.0	10	1	1923 ± 27	6.8 ± 0.4	98.76 ± 4.3
F2G3	1.2	10	1	2497 ± 31	5.9 ± 0.7	98.11 ± 3.8

**X-ray Diffraction (XRD).** The crystallinity of free SLM was assessed by XRD after the formation of the inclusion complex (F2). The free SLM and F2 were scanned between 2theta values of 5–60 °C using a diffractometer (Rigaku, Tokyo Japan).

**Formulation of Silymarin Inclusion Complex-Based Gels.** The selected inclusion complex (F2) was further converted to a Carbopol-based gel (Table 2). Three concentrations of Carbopol (F2G1 0.8%, F2G2 1.0%, F2G3 1.2% w/v) were taken and soaked overnight in distilled water for complete swelling. Carbopol solution was mixed with F2 with continuous stirring. The prepared sample was homogenized for uniform mixing to get a homogeneous gel formulation. Finally, the preservative (chlorocresol 1% w/v) and plasticizer PEG 200 (10% w/w) were added and pH was adjusted with triethanolamine.<sup>23</sup> The prepared different gels (F2G1, F2G2, and F2G3) have been further characterized below.

**Gel Characterization.** The prepared gels (F2G1, F2G2, and F2G3) were characterized for pH, clarity, viscosity, spreadability, and drug content. The clarity of the prepared gel was evaluated by a visual method. The samples were examined visually for the existence of any particles in the gel. A digital pH meter was used to measure the pH of the prepared gel. The viscosities of gels (F2G1, F2G2, F2G3) and SLM control gel (without CDs) were measured by a Brookfield viscometer (V420001, Fungi Lab, Spain). The spreadability was evaluated by taking the gel (1 g) and keeping it on the glass slide. The gel was covered with another glass slide, and constant weight was spread over it for 1 min. The weight was removed and the spread area was measured and noted.<sup>30</sup> The drug content was determined to evaluate the content uniformity of SLM. The gel (1 g) was taken in a volumetric flask, and methanol was added and then sonicated for a few minutes. The samples were vortexed for a few minutes for complete solubilization of SLM. The solution was collected, filtered, and diluted to determine the amount of SLM present in each formulation using a UV/visible spectrophotometer.

**Permeation Study.** The permeation study was done for the selected gel (F2G2) using the artificial synthetic membrane using the diffusion cell (area 1.2 cm<sup>2</sup>) with a diffusion volume (25 mL). The diffusion cell was assembled with the membrane fixed between the donor and receptor cells. The selected gel F2G2 and control SLM gel (1 g) were added to the donor cell and covered with aluminum foil. The study was performed at 37 °C and the diffusion media was stirred at 300 rpm. The permeated content (1 mL) was collected at different time points (0.5, 1, 2, 3, 4, 5, 6 h) and replenished with fresh blank media. The samples were filtered, and the diluted and the permeated SLM concentration at each time point was estimated by the reported HPLC method.<sup>31</sup> The concentration was used to calculate the amount of SLM permeated (%) and flux. The enhancement ratio was also calculated for F2G2 in comparison with the control SLM gel.

**Denaturation Assay.** The denaturation assay was carried out by bovine serum albumin following the slightly modified procedure.<sup>32</sup> The bovine serum solution (1%) was prepared

and added to 2.8 mL of PBS (pH 7.4). A two mL portion of each sample (free SLM and F2G2) was added at different concentrations (25–500 g/mL). The resulting mixtures were incubated for 15 min at 37 °C in a water bath and further heated at 70 °C for 5 min. After the mixtures were removed and kept aside for cooling, the turbidity of each was noted at 600 nm by using UV spectroscopy. The buffer (pH 7.4) was taken as the control, and the protein denaturation inhibition (%) was determined by using the subsequent formula

$$\text{inhibition (\%)} = 100 - \frac{x - y}{y} \times 100 \quad (3)$$

where  $x$ : sample absorbance and  $y$ : control absorbance.

**Antioxidant Activity.** A DPPH assay was carried out using the previously mentioned protocol with slight modification.<sup>33</sup> DPPH solution (0.004%) was prepared in methanol and kept in the dark. Separately different concentrations of free SLM and F2G2 were prepared in methanol. The DPPH solution (1.8 mL) was mixed with each concentration of test samples (0.2 mL). The mixtures were vortexed and kept aside at room temperature in the dark. The reaction mixture's absorbance was measured at 517 nm. Methanol and DPPH solution (without sample) were used as blank and control, respectively. The following formula was used to compute the scavenging activity

$$\text{scavenging activity (\%)} = \frac{x - y}{Y} \times 100 \quad (4)$$

where  $x$ : absorbance of the sample and  $y$ : absorbance of the control.

**Cell Viability Study.** The study is one of the primary assessments to evaluate the drug and its formulation to check the cytotoxicity.<sup>34</sup> The free SLM and F2G2 were taken in different concentrations (10–500 μg/mL) and treated with a skin cancer cell line (B16F10). It was employed to evaluate the effect of free SLM and F2G2 on cancer cells. The cells were grown using DMEM (with FBS 10%), streptomycin (100 mg/mL), and penicillin (100 units/mL). The cells were transferred to a 96-well plate and then incubated for 48 h at 37 °C with a continuous supply of CO<sub>2</sub> (5%) in an incubator. MTT solution was added to the well, and the mixture was further incubated for 3 h. The reagent was removed, DMSO (100 μL) added to it, and kept in an incubator for 30 min.<sup>35</sup> The absorbance was measured by using an ELISA microplate reader. The cell viability was calculated using the untreated cells as a control.

$$\text{cell viability (\%)} = \frac{x}{y} \times 100 \quad (5)$$

where  $x$ : treated cells' absorbance and  $y$ : untreated cells' absorbance.

**Molecular Docking.** The smiles notation of SLM was retrieved from Pubchem,<sup>36</sup> which was further changed into pdbqt (Protein Data Bank, partial charge (Q), and atom type (T) format) to generate the 3D structure by using the software Open Babel GUI. The PDB files of the X-ray crystal structure of tubulin-colchicine receptor (PDB ID: 1SAO) and β amylose/

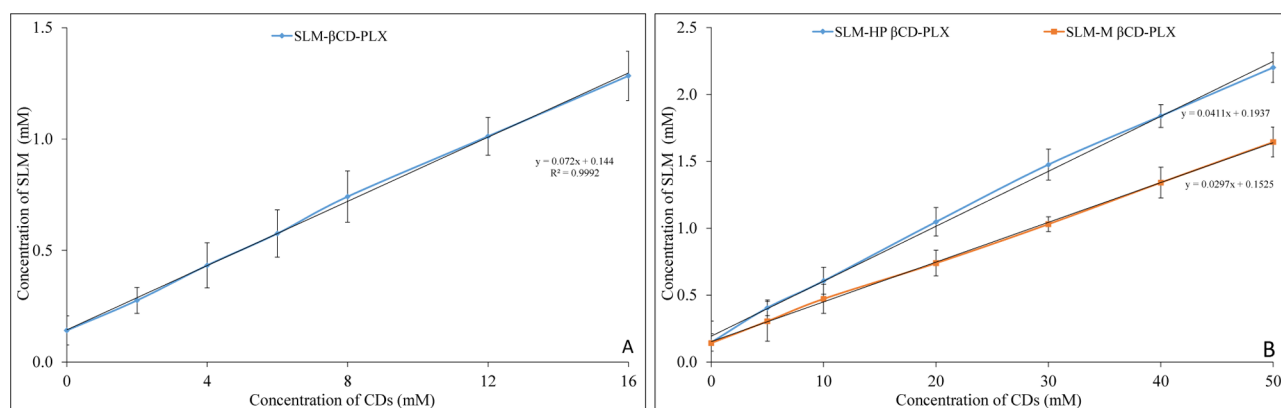


**Figure 3.** Phase solubility study of SLM with (A)  $\beta$ CD-PLX, (B) HP  $\beta$ CD-PLX; M- $\beta$ CD-PLX. The study was performed in triplicate ( $n = 3$ ) and data shown as mean  $\pm$  SD.

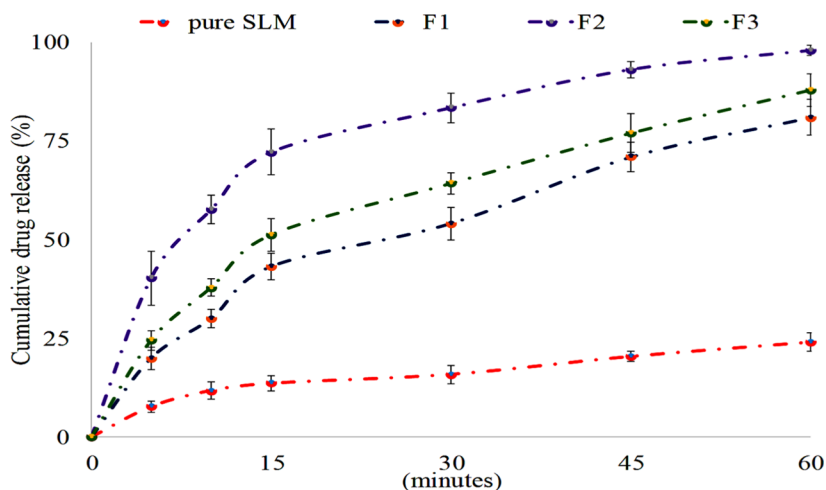


**Figure 4.** Comparative release profile of free SLM and SLM inclusion complexes (F1, F2, F3). The study was performed in triplicate ( $n = 3$ ) and data shown as mean  $\pm$  SD.

$\beta$  CD complex (PDB ID: 1BFN) were extracted from the RCSB Protein Data Bank (<https://www.rcsb.org/>). The tubulin-colchicine receptor possesses A, B, C, D, and E chains. The literature suggests that out of the five chains, the colchicine binding site is at the junction of the A and B chains of tubulin.<sup>37</sup> Hence, we choose the A and B chains of the tubulin receptor for our study. The beta-CD lies on chain B of the complex. Therefore, we restored  $\beta$ CD from chain B for our investigation. The structure of HP  $\beta$ CD and M  $\beta$ CD was built manually by appending isopropyl and methyl moiety on the retrieved structure of  $\beta$  CD with the help of the software PyMOL 2.4.0. The pdb file of the downloaded receptors was further processed and optimized using auto dock tools (ADT) version 1.5.6 ([www.autodock.scrips.edu](http://www.autodock.scrips.edu); La Jolla, CA, USA). The dimensions of the grid box for the tubulin receptor were set at 126 points for each coordinate and the center of the box was set at 122.884, 92.591, and 5.46 for  $x$ ,  $y$ , and  $z$  coordinates, respectively. For the three complexing agents ( $\beta$  CD, HP  $\beta$ CD, M  $\beta$ CD), the dimensions (grid size) and grid centers were kept the same. The grid points (size) were set at 32, 26, and 34, whereas the grid center was set at  $-6.962$ ,  $28.381$ , and  $29.995$  for  $x$ ,  $y$ , and  $z$  coordinates. The active torsion was set at 9 for SLM when docked with both receptors. The Lamarckian genetic algorithm with 10 runs was performed to obtain the best lowest energy-bound state. The protein was prepared and optimized by ADT version 1.5.6 ([www.autodock.scrips.edu](http://www.autodock.scrips.edu); La

Jolla, CA, USA). The docking score and docked 3D poses of the protein–ligand were assessed and visualized by using PyMOL 2.4.0 and ADT. The schematic 2D structure of SLM,  $\beta$ CD, and M  $\beta$ CD was illustrated from the software BIOVIA Discovery Studio, 2024. HP  $\beta$ CD's 2D schematic structure was drawn by the Chem3D 14.0 suite (77 fourth Avenue, Waltham, MA 02451). The validation of the final complex was performed by running MolProbity (<http://molprobity.biochem.duke.edu/>).

**Statistical Analysis.** All the studies were performed in triplicate ( $n = 3$ ) and data shown as mean  $\pm$  SD. One-way ANOVA was performed to check the statistical difference, and  $p$  value  $< 0.05$  was considered as significant.

## RESULTS AND DISCUSSION

**Phase Solubility.** The phase solubility study was performed to evaluate the stability constant and complexation efficiency of SLM with  $\beta$ CD-PLX, HP  $\beta$ CD-PLX, and M  $\beta$ CD-PLX. The graph was plotted between SLM and CDs-PLX concentrations as shown in Figure 3A and B. The graph was found to be linear with an increase in the CDs concentration leading to a gradual enhancement in SLM solubility as previously reported in the literature.<sup>7,9</sup> The stability constant (Ks) was calculated for each sample, and the values were found to be  $548 \text{ M}^{-1}$  ( $\beta$ CD-PLX),  $736 \text{ M}^{-1}$  (M  $\beta$ CD-PLX), and  $911$

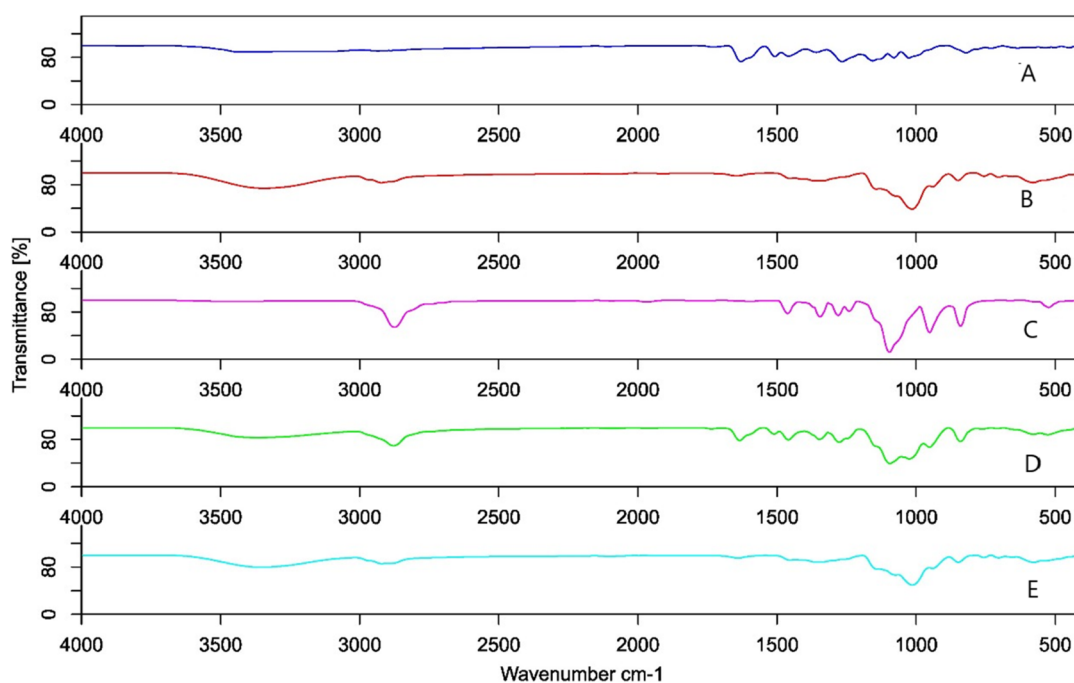


**Figure 5.** IR spectra of (A) free SLM; (B) HP  $\beta$ CD; (C) Poloxamer 188; (D) SLM PM; (E) SLM ICs (F2).

$M^{-1}$  (HP  $\beta$ CD-PLX), respectively. The trend in binding constant values showed that HP  $\beta$ CD-PLX exhibited the highest stability constant followed by  $\beta$ CD-PLX and M  $\beta$ CD-PLX. The stability constant value was found to be higher than the previously reported combination of SLM with  $\beta$ CD-TPGS.<sup>9</sup> Among all CDs, HP  $\beta$ CD has shown the maximum solubility effect and the higher stability constant value indicates a strong tendency of the guest molecules to be included in the interior of CD taurus.<sup>38,39</sup> CE was calculated from the slope value, and it shows 0.027, 0.038, and 0.045 for  $\beta$ CD, M  $\beta$ CD, and HP  $\beta$ CD, respectively. The inclusion complex prepared with HP  $\beta$ CD-PLX displayed significantly better results than those with  $\beta$ CD-PLX and M  $\beta$ CD-PLX.

**Dissolution Study.** The enhancement in the release pattern of the SLM inclusion complex using  $\beta$ CD-PLX (F1), HP  $\beta$ CD-PLX (F2), and M  $\beta$ CD-PLX (F3) was established by the dissolution study, and data are shown in Figure 4. The free SLM displayed a poor drug release with a maximum release of  $24.1 \pm 2.4\%$  in 60 min due to its poor solubility. This type of release was also reported in the literature.<sup>8</sup> The release rate of inclusion complex (F1, F2, F3) prepared with different CDs was higher ( $p < 0.001$ ) than that of free SLM. In the case of inclusion complex F1, it demonstrated a significant ( $p < 0.001$ ) enhancement in the release pattern with a release of  $80.9 \pm 4.6\%$ . The inclusion complex F2, shows the maximum release of  $97.9 \pm 3.8\%$ , followed by the inclusion complex F3, which showed the release of  $87.9 \pm 4.1\%$ . The release pattern from the prepared inclusion complex was found to be in the order  $F2 < F3 < F1$ . In the initial 10 min study, the release patterns were also found to be significantly different from each other:  $F2 (57.6 \pm 3.7\%) > F3 (37.9 \pm 2.3\%, p < 0.01), > F1 (30.2 \pm 2.3\%; p < 0.001)$ . Among the used CDs, HP  $\beta$ CD showed the quickest release because it offers several advantages like enhanced water solubility, high absorption, and bioavailability. So, it is frequently used as a solubilizer or as an excipient in delivery systems.<sup>40,41</sup> The enhancement in the release was found due to the improvement in drug wettability, solubility,

and coexistence of SLM and CDs in the dissolution media.<sup>42</sup> CDs have surfactant-like properties owing to the hydrophilicity toward the exterior side and reduce the interfacial tension between the poorly soluble drug and the release medium.<sup>43</sup> The drug molecules enclosed inside the CD torus may have contributed to faster drug release from inclusion complexes. It may add hydrophilic qualities and make the substance more soluble and wettable.<sup>44</sup> The transformation of SLM into a highly energetic amorphous state, followed by a decrease in crystallinity after complexation, may also be the cause of the improvement in dissolution rate.<sup>45</sup>

The release data were fitted to different release kinetics parameters, and the inclusion complex showed the Korsmeyer peppas model (regression value [0.9895 (F1), 0.9681 (F2), 0.9973 (F3)]). Further, the samples were evaluated for mean dissolution time (MDT), dissolution efficiency (DE), mean residence time (MRT), the area between the drug dissolution curve and its asymptote (ABC), and relative dispersion of dissolution time (RD). Among these inclusion complexes, F2 displayed a significant ( $p < 0.001$ ) difference in the MDT and MRT parameters than F2 and F1. MDT and MRT were found to be lowest for F2 (13.25, 14.86 min), followed by F3 (19.53; 20.49 min), and F1 (20.89; 21.64 min). F2 showed about 1.5–1.7-fold lesser MDT than inclusion complexes F1 and F3. The minimum MDT and MRT values give a quicker dissolution time in the used media. For the other factors such as DE and RD, F2 displayed a significant difference in the results than F1 and F3. The maximum DE was found to be 0.7625% for F2, followed by F3 (0.5926%) and F1 (0.5272%). A nonsignificant difference in the DE was observed between the samples F1 and F3.

**Infrared Spectroscopy.** The interpretation of the IR vibrations represents the frequency of the free SLM, carriers (HP  $\beta$ CD and PLX) along with the physical mixture, and F2, as depicted in Figure 5. SLM exhibits phenolic hydroxyl group ( $-\text{OH}$ ) stretching at  $3420.78 \text{ cm}^{-1}$  and C–H stretching vibration at  $2934.79 \text{ cm}^{-1}$ . The carbonyl group vibration peak

was obvious at  $1629.98\text{ cm}^{-1}$ , whereas the C–O–C peak was exhibited at  $1459.11\text{ cm}^{-1}$ .<sup>46</sup> The carrier HP  $\beta$ CD and PLX exhibited their hydroxyl stretching peak at  $3344.06\text{ cm}^{-1}$ , C–O–C stretching peak at  $1014.85\text{ cm}^{-1}$ , and vibrational stretching peaks at  $2874.93$  and  $1095.89\text{ cm}^{-1}$  for the OH and C–O–C moiety, respectively. Further, the vibrational peak of the physical mixture shows various changes in the frequencies of SLM and carriers. It was observed that a merged stretching vibrational peak at  $3360.80\text{ cm}^{-1}$  was seen for both the phenolic hydroxyl group of SLM and the carriers. The OH stretching vibration with a slight change in the peak value was also observed for the PLX spectra at  $2878.11\text{ cm}^{-1}$ . In the case of SLM IC (F2), C–O–C peak values of the SLM, PLX, and HP  $\beta$ CD were prominent at  $1459.73$ ,  $1094.08$ , and  $1025.29\text{ cm}^{-1}$ , respectively. The merged peaks were observed at  $3351.12\text{ cm}^{-1}$  with a slight change in their frequency values for the free SLM and HP  $\beta$ CD. The merged C–H stretching peak was also observed at  $2920.32\text{ cm}^{-1}$  for the free SLM and carrier. This peak was not visible for the physical mixture, which may predict the formation of an inclusion complex. The C–O–C stretching frequency for the SLM and HP  $\beta$ CD with a slight change in their peak values was exhibited at  $1454.68$  and  $1013.35\text{ cm}^{-1}$ . The noticeable change in their frequency values for the formulation confirms the formation of the inclusion complex.

**Differential Scanning Calorimetry.** The calorimetry study was used to assess the thermal behavior of the free SLM after inclusion into the CD (Figure 6). The free SLM

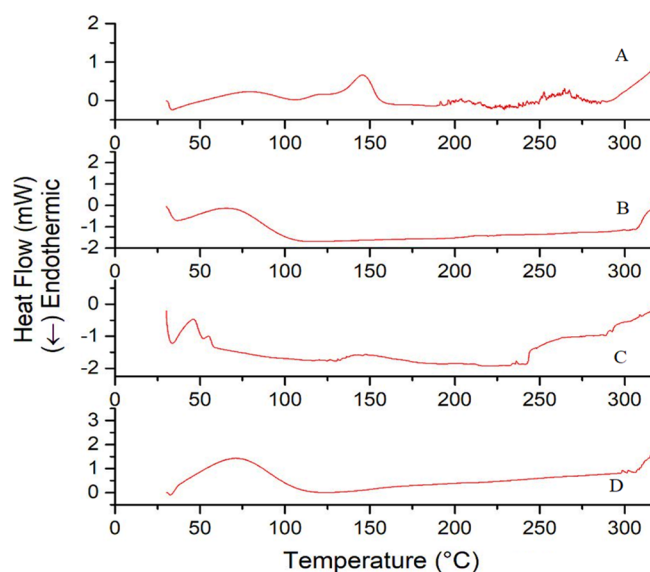


**Figure 6.** DSC thermogram of (A) free SLM; (B) HP  $\beta$ CD; (C) SLM PM; (D) SLM ICs (F2).

depicted the melting point at  $143.3\text{ }^{\circ}\text{C}$ , which is closer to the reported melting point.<sup>45</sup> The thermogram of HP  $\beta$ CD depicted a broad endotherm peak ranging from  $50$  to  $100\text{ }^{\circ}\text{C}$ , which is due to the loss of water molecules in the cavity of HP  $\beta$ CD.<sup>47</sup> In the case of inclusion complex (F2), there was a marked decrease in the intensity of the SLM melting peak. The results reveal stronger thermal stability in the formed complex compared to the drug, likely due to the cavity matching between SLM and HP  $\beta$ CD. The absence of the drug melting effect observed in the complex is an indication of strong interactions in the solid state, and complete drug amorphiza-

tion occurs after the formation of the complex. A similar type of observation was previously reported for another drug.<sup>48</sup>

**Scanning Electron Microscopy.** Figure 7 illustrates the morphological evaluation of the various samples (free SLM and inclusion complex, F2) using SEM analysis. The free SLM particles had smooth surfaces and resembled oblong polyhydric crystals. There was a noticeable alteration in the shape of the free SLM in the freeze-dried inclusion complex (F2). The individual components could no longer be distinguished from one another, only uneven and amorphous formed particles were observed. SEM and DSC results displayed homogeneous amorphous systems prepared by the freeze-drying method.

**X-ray Diffraction Study.** Figure 8 displays the diffraction pattern of free SLM and inclusion complex (F2) to assess the change in SLM crystallinity after the formation of the inclusion complex. The free SLM depicted high-intensity peak at  $2\theta$  values of  $14.58$  ( $318$ ),  $19.66$  ( $283$ ),  $24.54$  ( $262$ ),  $38.8$  ( $5482$ ),  $44.28$  ( $2364$ ),  $77.52$  ( $945$ ),  $81.68$  ( $577$ ),  $110.9$  ( $224$ ), and  $115.38$  ( $212$ ). In the case of the inclusion complex (F2), the peak intensity significantly reduced at  $14.66$  ( $83$ ),  $24.34$  ( $116$ ),  $38.8$  ( $3730$ ),  $44.26$  ( $1293$ ),  $77.5$  ( $606$ ),  $81.68$  ( $454$ ),  $110.9$  ( $189$ ), and  $115.38$  ( $116$ ). The peak intensities are significantly reduced and merged with adjacent peaks due to the presence of CDs as carriers in the inclusion complex. SLM is enclosed in the cavity of CDs and confirms the formation of the inclusion complex. The formation of complex leads to the conversion of SLM to an amorphous form, which is beneficial for increasing its solubility.<sup>8</sup>

**Gel Characterization.** The prepared SLM IC gels (F2G1, F2G2, F2G3) were evaluated for clarity, viscosity, pH, and spreadability studies (Table 2). The three different types of SLM IC gels were prepared using varying concentrations of Carbopol, and their viscosities were measured. The viscosity was found in the range of  $1787 \pm 22$ – $2497 \pm 31\text{ cP}$ . A digital pH meter used to determine the pH and the results revealed no significant differences ( $p > 0.05$ ) in the prepared compositions. The developed gels showed spreadability results in the following order: F2G1 ( $7.4\text{ cm}^2$ ) > F2G2 ( $6.8\text{ cm}^2$ ) > F2G3 ( $5.9\text{ cm}^2$ ). The drug content of the SLM IC gels was determined, and the result showed a drug content between  $98.11 \pm 3.8$  and  $99.43 \pm 3.4\%$ . Finally, the optimized gel formulation F2G2 was selected for further study. It showed a pH of  $6.5 \pm 0.3$ , a viscosity of  $1923 \pm 27\text{ cP}$ , a drug content of  $98.76 \pm 4.3\%$ , and a spreadability of  $6.8 \pm 0.4\text{ cm}^2$ . With the variation in the Carbopol concentration, a significant change in viscosity takes place. Previous reports of gel formulations observed a similar type of results.<sup>49,50</sup> The viscosity of the gel also influences its spreadability; an increase in Carbopol concentration leads to a decrease in spreadability. Finally, the optimal gel (F2G1) was selected based on its viscosity and spreadability over the other formulations.

**Permeation Study.** The study was performed to check the permeation of SLM from a Carbopol-based gel system. F2G2 was evaluated and the result was compared with the control SLM gel. There is a significant ( $p < 0.001$ ) difference in the permeation of SLM observed from F2G2 than the control SLM gel. An enhanced SLM permeation flux ( $65.25 \pm 4.1\text{ }\mu\text{g cm}^2/\text{h}$ ) was found from F2G2, whereas the control SLM gel depicted only a flux value of  $17.25 \pm 2.9\text{ }\mu\text{g cm}^2/\text{h}$ . The permeability coefficient was found to be  $0.065252\text{ cm/h}$  and  $0.0172\text{ cm/h}$ , respectively. The enhancement ratio was calculated and about 3.7-fold enhancement in the SLM

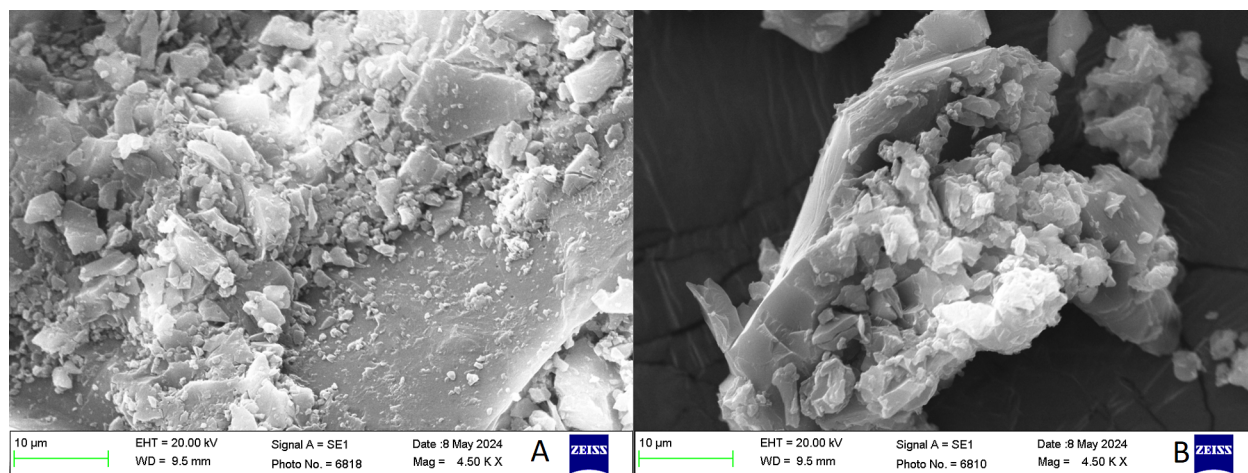


Figure 7. SEM image of (A) free SLM; (B) SLM ICs (F2).

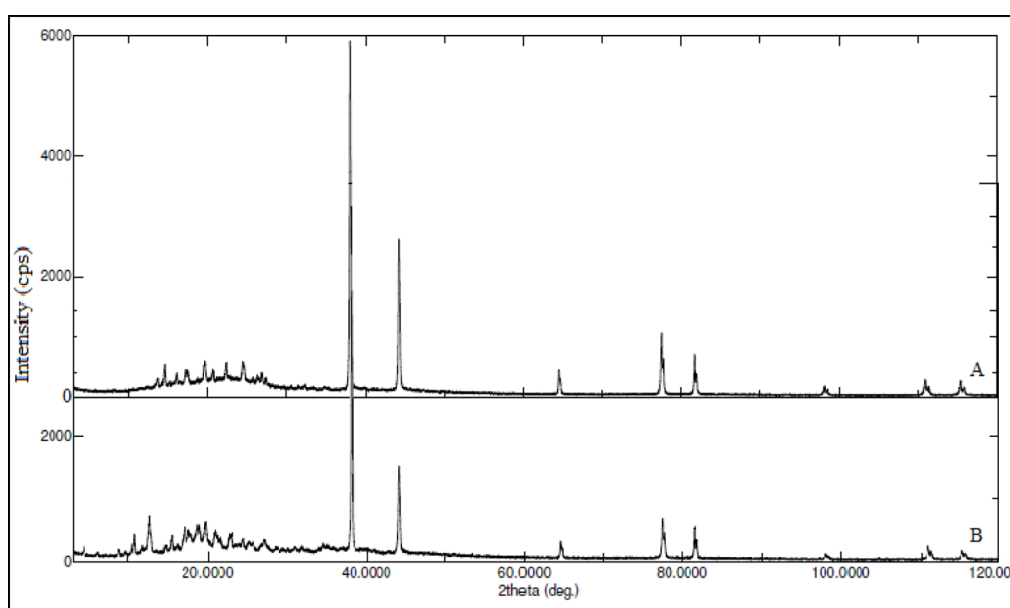


Figure 8. XRD of (A) free SLM and (B) SLM ICs (F2).

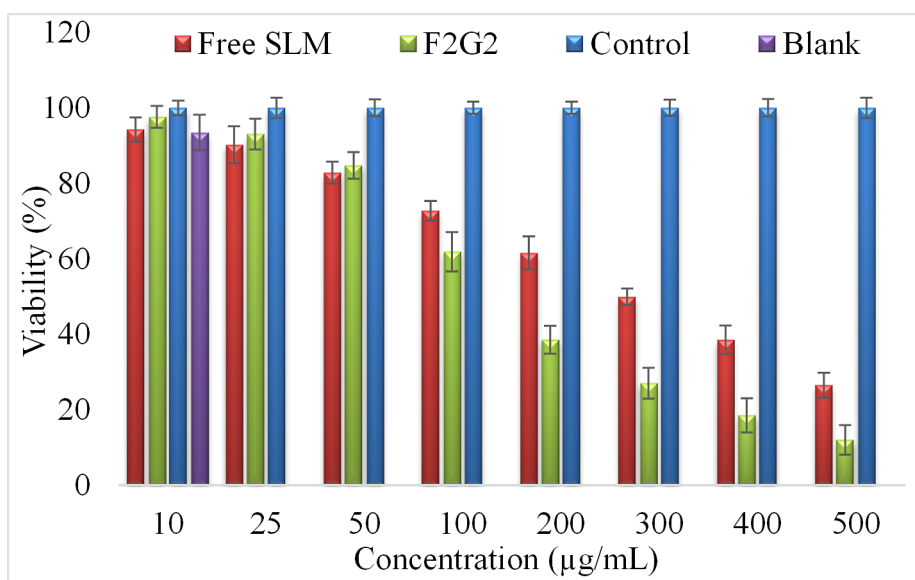
permeation was observed than for the control SLM gel. The primary reason for the enhancement in permeation is due to the capacity to penetrate membrane pores easily. The permeation of SLM through the membrane from F2G2 exhibited a statistically significant increase as compared to the control gel. It possesses the ability to traverse the membrane due to the presence of surfactant. It helps to solubilize the drug and promotes the permeation. They also possess the potential to attach for prolonged time to the membrane and it improves the permeation across the membrane.<sup>50</sup>

**Denaturation Assay.** The inflammatory precursors are secreted more readily during acute inflammation in cancer. The plasma concentration of inflammatory mediators rises during this time.<sup>51</sup> Bovine serum albumin is a protein that is frequently found in blood plasma. It loses its biological characteristics after denaturation because it loses its original structure.<sup>52</sup> This test was selected and carried out to assess the potential of free SLM and F2G2 at various concentrations (25–500 g/mL). The findings show that the levels of protein denaturation in both samples decreased with the concen-

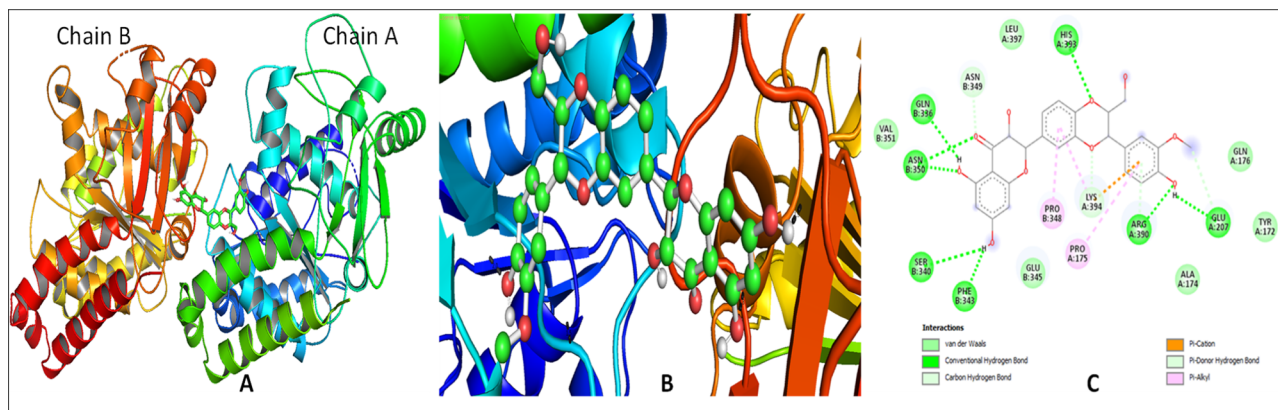
tration. F2G2 showed  $65.2 \pm 3.4$ – $88.3 \pm 4.1\%$  suppression of albumin denaturation and free SLM showed  $69.6 \pm 3.7$ – $91.2 \pm 3.9\%$  inhibition. Furthermore, no discernible difference in protein denaturation inhibition was observed. F2G2 can prevent protein denaturation and would undoubtedly play a role in inflammation linked to skin cancer.

**Antioxidant Study.** The activity has been assessed for F2G2 and the results were compared with the free SLM and standard ascorbic acid (control). The standard ascorbic acid showed an antioxidant activity of  $18.3 \pm 1.7\%$  at  $10 \mu\text{g/mL}$ ,  $58.6 \pm 2.4\%$  at  $50 \mu\text{g/mL}$ , and  $91.4 \pm 3.9\%$  at  $100 \mu\text{g/mL}$ . Free SLM had shown significantly lower antioxidant activity of  $11.6 \pm 2.2\%$  at  $10 \mu\text{g/mL}$ ,  $41.3 \pm 3.9\%$  at  $50 \mu\text{g/mL}$ , and  $67.4 \pm 4.5\%$  at  $100 \mu\text{g/mL}$  than ascorbic acid. F2G2 displayed a greater potential for antioxidant activity. It depicted  $17.6 \pm 3.1\%$  at  $10 \mu\text{g/mL}$  ( $p < 0.001$ ),  $54.1 \pm 2.9\%$  at  $50 \mu\text{g/mL}$  ( $p < 0.001$ ), and  $87.3 \pm 4.2\%$  at  $100 \mu\text{g/mL}$  ( $p < 0.001$ ). After the preparation of F2G2, the activity increased by about 1.2–1.6-fold compared to the free SLM solution. Better solubility of SLM after encapsulation into the inclusion complex led to enhanced activity.

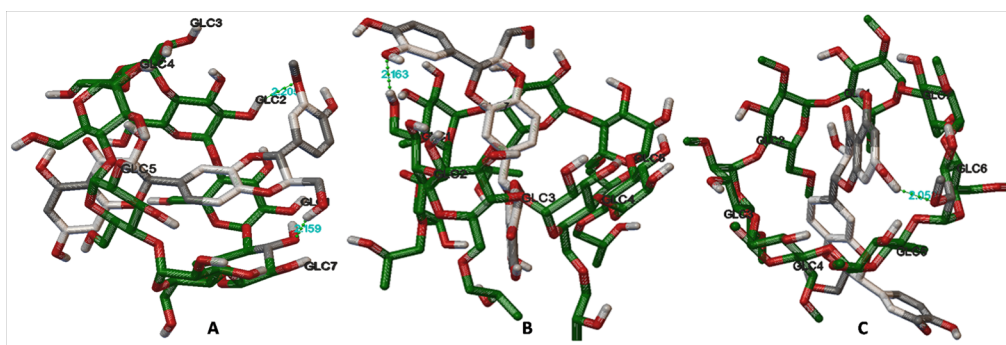




**Figure 9.** Cell viability assay results of blank (carrier only), control (not treated), free SLM, and SLM ICs gel (F2G2). A triplicate study was performed and data shown as mean  $\pm$  SD.



**Figure 10.** Molecular docking of (A) docked pose of SLM (ball and stick in green) with a receptor in ribbon. (B) Zoom view of H-bond interaction (black dotted line) of SLM with the receptor (software: PyMOL 2.4.0). (C) 2D docking interaction of the drug with the receptor (software: BIOVIA Discovery Studio, 2024).

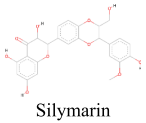


**Figure 11.** Docked pose of SLM (ligand) with complexing agents (A)  $\beta$ CD, (B) HP  $\beta$ CD, (C) M  $\beta$ CD representing H-bond interaction in the ball and stick model; complexing agents: green color; SLM: ash gray (software: AutoDock Tools-1.5.6; [www.autodock.scrips.edu](http://www.autodock.scrips.edu); La Jolla, CA, USA).

**Cell Viability Study.** The assay was performed for the skin cancer cell line, and the comparative result is shown in Figure 9. The study was performed between 10 and 500  $\mu$ g/mL and results displayed a concentration-dependent activity. The increase in SLM concentration and greater activity were achieved from both free SLM and F2G2. A nonsignificant

difference was observed at the initial concentration (10, 25, 50  $\mu$ g/mL). At these initial concentrations, free SLM showed slightly higher activity than F2G2. A significantly lesser activity was achieved from free SLM at 100  $\mu$ g/mL ( $72.72 \pm 6.2\%$ ;  $p < 0.05$ ), 200  $\mu$ g/mL ( $61.57 \pm 5.4\%$ ;  $p < 0.001$ ), 300  $\mu$ g/mL ( $49.95 \pm 7.3\%$ ;  $p < 0.001$ ), 400  $\mu$ g/mL ( $38.53 \pm 3.9\%$ ;  $p <$

Table 3. Binding Energy, Hydrogen Bond Distance, and Interaction of SLM with the Receptors

Ligand	Receptors	Free binding energy (Kcal/mol)	No. of H-bond	Distance of H-bond (Å)	Amino acid residue (Receptor)	Structural features (Ligand: Silymarin)
 Silymarin	α,β-Tubulin-colchicine receptor	-6.28	4	1.926	PHE 343	C-7 Hydrogen of hydroxyl moiety of chromene ring
				2.008	ARG 390	C-20 oxygen of hydroxyl moiety of phenyl ring
				2.104	ASN 350	C-5 oxygen of hydroxyl moiety of chromene ring
				2.188	GLU 207	C-20 Hydrogen of hydroxyl moiety of phenyl ring
	βCD	-4.61	2	2.159	C-3 oxygen of hydroxyl moiety at GLC 7	C-23 hydrogen of hydroxy methyl moiety
				2.205	C-2 hydrogen of hydroxyl moiety at GLC 2	C-19 Oxygen of methoxyphenyl moiety
	HP βCD	-5.77	1	2.163	C-3 hydrogen of hydroxyl moiety at GLC 2	C-19 Oxygen of methoxyphenyl moiety
	M βCD	-5.61	1	2.052	C-3 oxygen of hydroxyl moiety at GLC 6	C-7 Hydrogen of hydroxyl group of chromene ring

0.001), and 500  $\mu\text{g}/\text{mL}$  ( $26.54 \pm 2.7\%$ ;  $p < 0.001$ ). In the case of F2G2, it showed higher activity at 100  $\mu\text{g}/\text{mL}$  ( $61.86 \pm 4.9\%$ ), 200  $\mu\text{g}/\text{mL}$  ( $38.55 \pm 4.2\%$ ), 300  $\mu\text{g}/\text{mL}$  ( $27.04 \pm 2.9\%$ ), 400  $\mu\text{g}/\text{mL}$  ( $18.55 \pm 3.2\%$ ), and 500  $\mu\text{g}/\text{mL}$  ( $12.04 \pm 1.9\%$ ;  $p < 0.001$ ). There were about 1.2-fold (100  $\mu\text{g}/\text{mL}$ ), 1.6-fold (200  $\mu\text{g}/\text{mL}$ ), 1.9-fold (300  $\mu\text{g}/\text{mL}$ ), 2.1-fold (400  $\mu\text{g}/\text{mL}$ ), 2.2-fold (500  $\mu\text{g}/\text{mL}$ ) enhancements in the activity from F2G2. The free SLM showed the  $\text{IC}_{50}$  value of  $304.7 \pm 5.7 \mu\text{g}/\text{mL}$  and F2G2 showed  $145.3 \pm 4.2 \mu\text{g}/\text{mL}$ . There was a 2.1-fold reduction in the  $\text{IC}_{50}$  value achieved from F2G2. The blank sample (without drug) was also assessed and it showed the cell viability of  $93.45 \pm 4.7\%$  activity. SLM can get rid of reactive oxygen species, which cause most of the oxidative damage in living things. Because of this, it can protect against diseases linked to oxidative damage and UVB skin conditions caused by radiation. The enhancement in the activity was achieved due to the increase in the SLM solubility, which led to an increase in the drug permeability. The higher intercellular uptake of SLM into the cancer cells causes a reduction in cell viability. The findings of the study support the previously published literature.<sup>52</sup>

**Molecular Docking.** SLM is a plant-derived flavonoid obtained from the fruits and seeds of milk thistle belonging to the family Asteraceae. The previous findings highlighted that it possesses a chemopreventive effect. It is pharmacologically safe and can be used for in vitro cell culture models of skin carcinogenesis.<sup>53</sup> The protein chosen for the drug to dock was a tubulin-colchicine receptor, and complexing agents are illustrated in Figures 10 and 11. Chemically, SLM is a flavonolignan, gripped as a small molecule to observe the interaction with the tubulin-colchicine receptor. The tubulin-colchicine receptor possesses five chains, viz., A, B, C, D, and E chains. It was further suggested through the literature that the ligand binds best at the synapse of the A–B subunit of the tubulin receptor.<sup>37</sup> Hence, the A and B chain of the tubulin receptor was restored to fetch for the lowest binding affinity and best-fitted docked poses. The docked poses (Figure 10A) furnish information about the durability of the drug and receptor genesis. The SLM and the tubulin receptor exhibited a docking score of  $-6.28$  kcal/mol. SLM forms four hydrogen bonds with the tubulin receptor (two H-bonds with chain A and two H-bonds with chain B; Figure 10B) with bond lengths of 1.926, 2.008, 2.104, and 2.188 Å, respectively. The stability of the docked structure was depicted by the formation of

hydrogen bonds (Figure 10C). The high docking score suggests the virtuous interaction of the drug at the active site of the colchicine-tubulin receptor.

SLM was also docked with the three-complexing agent ( $\beta\text{CD}$ , HP  $\beta\text{CD}$ , and M  $\beta\text{CD}$ ) to observe their binding affinity (Figure 11A–C). The binding score of SLM docked with  $\beta\text{CD}$  was found to be  $-4.61$  kcal/mol (Figure 11A). The drug formed two hydrogen bonds with a bond length of 2.159 and 2.205 Å, exhibiting its interaction with the complexing agent ( $\beta\text{CD}$  receptor). The HP  $\beta\text{CD}$  receptor interacted with SLM and exhibited the binding score of  $-5.77$  kcal/mol with the formation of one hydrogen bond at 2.163 Å (Figure 11B). The M  $\beta\text{CD}$  receptor depicted a binding score of  $-5.61$  kcal/mol after docking with SLM. This interaction leads to the formation of one hydrogen bond having a bond distance of 2.052 Å with the receptor (Figure 11C). The validity of the final complex was performed by the MolProbity and it showed 100th percentile with zero clash score for all atoms. The detailed summary of the docking study is outlined in Table 3. The above study concludes that the interaction of SLM with the colchicine-tubulin receptor and complexing agents exhibited a high docking score. This illustrates the commendable interaction of the drug with the receptors.

## CONCLUSIONS

In the present study, a CD-based inclusion complex was prepared by a freeze-drying method for the evaluation of complexing and solubilizing properties of SLM. FTIR, DSC XRD, and SEM studies confirm the inclusion of SLM into CD cavities. The dissolution study revealed enhanced solubility and drug release compared to free SLM. The molecular docking results support the findings of the formation of a stable inclusion complex with a higher binding energy score. Finally, the prepared SLM inclusion complex-based gel displayed optimum gel characterization, enhanced drug permeation, and antioxidant activity. The cell viability assay results demonstrated that F2G2 clearly showed in vitro cell viability higher than that of free SLM.  $\text{IC}_{50}$  was also calculated and found to be significantly lower for the F2G2 than free SLM. Based on the findings, we recommend the application of HP  $\beta\text{CD}$  for the delivery of poorly soluble bioactive compounds (SLM), which might warrant improved in vivo pharmacokinetics and further clinical success in cancer.

## AUTHOR INFORMATION

### Corresponding Authors

Syed Sarim Imam – Department of Pharmaceutics, College of Pharmacy, King Saud University, Riyadh 11451, Saudi Arabia; [orcid.org/0000-0002-8913-0826](https://orcid.org/0000-0002-8913-0826); Email: [simam@ksu.edu.sa](mailto:simam@ksu.edu.sa)

Sultan Alshehri – Department of Pharmaceutics, College of Pharmacy, King Saud University, Riyadh 11451, Saudi Arabia; [orcid.org/0000-0002-0922-9819](https://orcid.org/0000-0002-0922-9819); Email: [salshehri1@ksu.edu.sa](mailto:salshehri1@ksu.edu.sa)

### Authors

Wael A. Mahdi – Department of Pharmaceutics, College of Pharmacy, King Saud University, Riyadh 11451, Saudi Arabia; [orcid.org/0000-0002-7083-1753](https://orcid.org/0000-0002-7083-1753)

Abdulkarim Alotaibi – Department of Pharmaceutics, College of Pharmacy, King Saud University, Riyadh 11451, Saudi Arabia

Saad Alhallaf – Department of Pharmaceutics, College of Pharmacy, King Saud University, Riyadh 11451, Saudi Arabia

Riyad F. Alzhrani – Department of Pharmaceutics, College of Pharmacy, King Saud University, Riyadh 11451, Saudi Arabia

Complete contact information is available at:

<https://pubs.acs.org/10.1021/acsomega.4c09614>

### Notes

The authors declare no competing financial interest.

## ACKNOWLEDGMENTS

This research project is supported by Researchers Supporting Project number (RSP2025R146), King Saud University, Riyadh, Saudi Arabia.

## REFERENCES

- (1) Iqbal, B.; Ali, J.; Ganguli, M.; Mishra, S.; Baboota, S. Silymarin-loaded nanostructured lipid carrier gel for the treatment of skin cancer. *Nanomedicine* **2019**, *14* (9), 1077–1093.
- (2) Singh, P.; Arya, M.; Kanoujia, J.; Singh, M.; Gupta, K. P.; Saraf, S. A. Design of topical nanostructured lipid carrier of silymarin and its effect on 7, 12-dimethylbenz [a] anthracene (DMBA) induced cellular differentiation in mouse skin. *RSC Adv.* **2016**, *6* (88), 84965–84977.
- (3) Kesharwani, S.; Jain, V.; Dey, S.; Sharma, S.; Mallya, P.; Kumar, V. A. An overview of advanced formulation and nanotechnology-based approaches for solubility and bioavailability enhancement of silymarin. *J. Drug Delivery Sci. Technol.* **2020**, *60*, 102021.
- (4) Yang, K. Y.; Hwang, D. H.; Yousaf, A. M.; Kim, D. W.; Shin, Y. J.; Bae, O. N.; Kim, Y.; Kim, J. O.; Yong, C. S.; Choi, H. G. Silymarin-loaded solid nanoparticles provide excellent hepatic protection: physicochemical characterization and in vivo evaluation. *Int. J. Nanomed.* **2013**, *8*, 3333–3343.
- (5) Gharbia, S.; Balta, C.; Herman, H.; Rosu, M.; Varadi, J.; Bacskay, I.; Vecsernyes, M.; Gyongyosi, S.; Fenyvesi, F.; Voicu, S. N.; Stan, M. S.; Cristian, R. E.; Dinischiotu, A.; Hermenean, A. Enhancement of Silymarin Anti-fibrotic Effects by Complexation With Hydroxypropyl (HPBCD) and Randomly Methylated (RAMEB)  $\beta$ -Cyclodextrins in a Mouse Model of Liver Fibrosis. *Front. Pharmacol.* **2018**, *9*, 883.
- (6) Mehraban, S.; Feily, A. Silymarin in Dermatol.: A Brief Review. *J. Pigment. Disord.* **2014**, *1* (4), 1–4.
- (7) Shankar, V. K.; Police, A.; Ajjarapu, S.; Murthy, S. N. Development of silymarin topical formulation: In vitro and ex vivo dermal kinetics of silymarin. *Int. J. Pharm.* **2023**, *630*, 122431.
- (8) Montecinos, F.; Sackett, D. L. Structural Changes, Biological Consequences, and Repurposing of Colchicine Site Ligands. *Biomolecules* **2023**, *13*, 834.
- (9) Donthiboina, K.; Anchi, P.; Gurram, S.; Sai Mani, G.; Lakshmi Uppu, J.; Godugu, C.; Shankaraiah, N.; Kamal, A. Synthesis and biological evaluation of substituted N-(2-(1H-benzo[d]imidazole-2-yl) phenyl) cinnamides as tubulin polymerization inhibitors. *Bioorg. Chem.* **2020**, *103*, 104191.
- (10) Chen, Z.; Gao, W.; Feng, X.; Zhou, G.; Zhang, M.; Zeng, L.; Hu, X.; Liu, Z.; Song, H. A comparative study on the preparation and evaluation of solubilizing systems for silymarin. *Drug Del. Transl. Res.* **2024**, *14*, 1616–1634.
- (11) Imam, S. S.; Alshehri, S.; Altamimi, M. A.; Mahdi, W. A.; Qamar, W. Formulation of Silymarin- $\beta$  Cyclodextrin-TPGS Inclusion Complex: Physicochemical Characterization, Molecular Docking, and Cell Viability Assessment against Breast Cancer Cell Lines. *ACS Omega* **2023**, *8* (38), 34898–34907.
- (12) Figueiras, A.; Ribeiro, L.; Vieira, M. T.; Veiga, F. Preparation and physicochemical characterization of omeprazole:methyl-beta-cyclodextrin inclusion complex in solid state. *J. Inclusion Phenom. Macrocyclic Chem.* **2007**, *57*, 173–177.
- (13) Zeng, Q. P.; Liu, Z. H.; Huang, A. W.; Zhang, J.; Song, H. T. Preparation and characterization of silymarin synchronized-release microporous osmotic pump tablets. *Drug Des., Dev. Ther.* **2016**, *10*, 519–531.
- (14) Yousaf, A. M.; Malik, U. R.; Shahzad, Y.; Mahmood, T.; Hussain, T. Silymarin-laden pvp-peg polymeric composite for enhanced aqueous solubility and dissolution rate: Preparation and in vitro characterization. *J. Pharm. Anal.* **2019**, *9* (1), 34–39.
- (15) Dai, K.; Wu, J.; Liu, X.; Wang, S.; Liu, Y.; Li, H.; Wang, H. Inclusion complex of quercetin with sulfobutylether  $\beta$ -cyclodextrin: preparation, characterization, antioxidant and antibacterial activities and the inclusion mechanism. *RSC Adv.* **2024**, *14*, 9472–9481.
- (16) Bera, H.; Chekuri, S.; Sarkar, S.; Kumar, S.; Muvva, N. B.; Mothe, S.; Nadiampalli, J. Novel pimozone- $\beta$ -cyclodextrin-polyvinylpyrrolidone inclusion complexes for Tourette syndrome treatment. *J. Mol. Liq.* **2016**, *215*, 135–143.
- (17) Stella, V. J.; Rajewski, R. A. Sulfobutylether- $\beta$ -cyclodextrin. *Int. J. Pharm.* **2020**, *583*, 119396.
- (18) Saffarionpour, S.; Diosady, L. L. Preparation and characterization of an iron- $\beta$ -cyclodextrin inclusion complex: factors influencing the host-guest interaction. *Food Funct.* **2023**, *14*, 5062–5077.
- (19) Jansook, P.; Kulsirachote, P.; Loftsson, T. Cyclodextrin solubilization of celecoxib: solid and solution state characterization. *J. Inclusion Phenom. Macrocyclic Chem.* **2018**, *90*, 75–88.
- (20) Srivalli, K. M. R.; Mishra, B. Improved Aqueous Solubility and Antihypercholesterolemic Activity of Ezetimibe on Formulating with Hydroxypropyl- $\beta$ -Cyclodextrin and Hydrophilic Auxiliary Substances. *AAPS PharmSciTech* **2016**, *17* (2), 272–283.
- (21) Wang, Y.; Deng, Z.; Wang, X.; Shi, Y.; Lu, Y.; Fang, S.; Liang, X. Formononetin/methyl- $\beta$ -cyclodextrin inclusion complex incorporated into electrospun polyvinyl-alcohol nanofibers: Enhanced water solubility and oral fast-dissolving property. *Int. J. Pharm.* **2021**, *603*, 120696.
- (22) Duarte, A.; Martinho, A.; Luis, A.; Figueiras, A.; Oleastro, M.; Domingues, F. C.; Silva, F. Resveratrol encapsulation with methyl- $\beta$ -cyclodextrin for antibacterial and antioxidant delivery applications. *LWT-Food Sci. Technol.* **2015**, *63* (2), 1254–1260.
- (23) Kalam, M. A.; Ali, R.; Alhowyan, A.; Ahmad, A.; Iqbal, M.; Raish, M. Quercetin-loaded transliposomal gel for effective management of skin cancer: In vitro and cell line efficacy studies. *J. Drug Delivery Sci. Technol.* **2024**, *96*, 105659.
- (24) Braga, S. S.; Pais, J. Getting under the skin: cyclodextrin inclusion for the controlled delivery of active substances to the dermis. In *Design of Nanostructures for Versatile Therapeutic Applications*; Grumezescu, A. M., Ed.; William Andrew Publishing, 2018; pp 407–449.

- (25) Sherje, A. P.; Londhe, V. Development and Evaluation of pH-Responsive Cyclodextrin-Based *in situ* Gel of Paliperidone for Intranasal Delivery. *AAPS PharmSciTech* **2018**, *19*, 384–394.
- (26) Higuchi, T.; Connors, K. A. Phase-solubility techniques. *Adv. Anal. Chem. Instrum.* **1965**, *4*, 117–212.
- (27) Suvarna, V.; Kajwe, A.; Murahari, M.; Pujar, G. V.; Inturi, B. K.; Sherje, A. P. Inclusion Complexes of Nateglinide with HP- $\beta$ -CD and L-Arginine for Solubility and Dissolution Enhancement: Preparation, Characterization, and Molecular Docking Study. *J. Pharm. Innov.* **2017**, *12*, 168–181.
- (28) Xu, D.; Li, X.; Huang, Y.; Tang, Z.; Ran, C.; Jing, B.; Yin, L.; Lin, J.; Fu, H.; Tang, H.; Zhao, X.; et al. Preparation, characterization and pharmacokinetic studies of sulfobutyl ether- $\beta$ -cyclodextrin-toltrazuril inclusion complex. *J. Mol. Struct.* **2021**, *1223*, 128969.
- (29) Chandra, A.; Ghate, M. V.; Aithal, K. S.; Lewis, S. A. In silico prediction coupled with *in vitro* experiments and absorption modeling to study the inclusion complex of telmisartan with modified beta-cyclodextrin. *J. Inclusion Phenom. Macrocyclic Chem.* **2018**, *91*, 47–60.
- (30) Raval, M.; Bagada, H. Formulation and Evaluation of Cyclodextrin-Based Thermosensitive *In Situ* Gel of Azithromycin for Periodontal Delivery. *J. Pharm. Innov.* **2021**, *16*, 67–84.
- (31) Petraskova, L.; Kanova, K.; Biedermann, D.; Kren, V.; Valentova, K. Simple and Rapid HPLC Separation and Quantification of Flavonoid, Flavonolignans, and 2,3-Dehydroflavonolignans in Silymarin. *Foods* **2020**, *9* (2), 116.
- (32) Gunathilake, K.; Ranaweera, K.; Rupasinghe, H. P. *In vitro* anti-inflammatory properties of selected green leafy vegetables. *Bio-medicines* **2018**, *6*, 107.
- (33) Sharma, O. P.; Bhat, T. K. DPPH antioxidant assay revisited. *Food Chem.* **2009**, *113* (4), 1202–1205.
- (34) Peram, M. R.; Jalalpure, S.; Kumbar, V.; Patil, S.; Joshi, S.; Bhat, K.; Diwan, P. Factorial design-based curcumin ethosomal nanocarriers for the skin cancer delivery: *in vitro* evaluation. *J. Liposome Res.* **2019**, *29* (3), 291–311.
- (35) Keshavarz, F.; Dorfaki, M.; Bardania, H.; Khosravani, F.; Nazari, P.; Ghalamfarsa, G. Quercetin-loaded Liposomes Effectively Induced Apoptosis and Decreased the Epidermal Growth Factor Receptor Expression in Colorectal Cancer Cells: An *In Vitro* Study. *Iran. J. Med. Sci.* **2023**, *48* (3), 321–328.
- (36) <https://pubchem.ncbi.nlm.nih.gov/>.
- (37) Choudhury, D.; Ganguli, A.; Dastidar, D. G.; Acharya, B. R.; Das, A.; Chakrabarti, G. Apigenin shows synergistic anticancer activity with curcumin by binding at different sites of tubulin. *Biochimie* **2013**, *95* (6), 1297–1309.
- (38) Salman, Z. N.; Al-Ani, I.; Al Azzam, K. M.; Majeed, B. J. M.; Abdallah, H. H.; Negim, E.-S. Enhancement of apixaban's solubility and dissolution rate by inclusion complex ( $\beta$ -cyclodextrin and hydroxypropyl  $\beta$ -cyclodextrin) and computational calculation of their inclusion complexes. *ADMET DMPK* **2023**, *11* (4), 533–550.
- (39) Haley, R. M.; Gottardi, R.; Langer, R.; Mitchell, M. J. Cyclodextrins in drug delivery: Applications in gene and combination therapy. *Drug Delivery Transl. Res.* **2020**, *10*, 661–677.
- (40) Naeem, A.; Yu, C.; Zhu, W.; Zang, Z.; Guan, Y. Study of Hydroxypropyl  $\beta$ -Cyclodextrin and Puerarin Inclusion Complexes Encapsulated in Sodium Alginate-Grafted 2-Acrylamido-2-Methyl-1-Propane Sulfonic Acid Hydrogels for Oral Controlled Drug Delivery. *Gels* **2023**, *9* (3), 246.
- (41) Ma, B.; Shen, Y.; Fan, Z.; Zheng, Y.; Sun, H.; Luo, J.; Wang, M. Characterization of the inclusion complex of 16,17 $\alpha$ -epoxyprogesterone with randomly methylated  $\beta$ -cyclodextrin in aqueous solution and in the solid state. *J. Inclusion Phenom. Macrocyclic Chem.* **2011**, *69*, 273–280.
- (42) Hirlekar, R. S.; Sonawane, S. N.; Kadam, V. J. Studies on the effect of water-soluble polymers on drug-cyclodextrin complex solubility. *AAPS PharmSciTec* **2009**, *10*, 858–863.
- (43) Nalluri, B. N.; Chowdary, K. P. R.; Murthy, K. V. R.; Hayman, A. R.; Becket, G. Physicochemical characterization and dissolution properties of nimesulide-cyclodextrin binary systems. *AAPS PharmSciTech* **2003**, *4*, No. E26.
- (44) Shalaby, K. S.; Ismail, M. I.; Lamprecht, A. Cyclodextrin Complex Formation with Water-Soluble Drugs: Conclusions from Isothermal Titration Calorimetry and Molecular Modeling. *AAPS PharmSciTech* **2021**, *22* (7), 232.
- (45) Lian, R.; Lu, Y.; Qi, J.; Tan, Y.; Niu, M.; Guan, P.; Hu, F.; Wu, W. Silymarin Glyceryl Monooleate/Poloxamer 407 liquid crystalline matrices: physical characterization and enhanced oral bioavailability. *AAPS PharmSciTech* **2011**, *12*, 1234–1240.
- (46) Venugopal, D. C.; Senthilnathan, R. D.; Maanvizi, S.; Madhavan, Y.; Sankarapandian, S.; Ramshankar, V.; Kalachaveedu, M. Preparation and Characterization of Silymarin Gel: A Novel Topical Mucoadhesive Formulation for Potential Applicability in Oral Pathologies. *Gels* **2023**, *9*, 139.
- (47) Ding, X.; Zheng, M.; Lu, J.; Zhu, X. Preparation and evaluation of binary and ternary inclusion complexes of fenofibrate/hydroxypropyl- $\beta$ -cyclodextrin. *J. Inclusion Phenom. Macrocyclic Chem.* **2018**, *91*, 17–24.
- (48) Gao, S.; Bie, C.; Ji, Q. Y.; Ling, H. Y.; Li, C. Y.; Fu, Y.; Zhao, L.; Ye, F. Preparation and characterization of cyanazine-hydroxypropyl-beta-cyclodextrin inclusion complex. *RSC Adv.* **2019**, *9* (45), 26109–26115.
- (49) Imam, S. S.; Gilani, S. J.; Zafar, A.; Jumah, M. N. B.; Alshehri, S. Formulation of Miconazole-Loaded Chitosan–Carbopol Vesicular Gel: Optimization to *In Vitro* Characterization, Irritation, and Antifungal Assessment. *Pharmaceutics* **2023**, *15*, 581.
- (50) Zheng, Y.; Ouyang, W.-Q.; Wei, Y.-P.; Syed, S. F.; Hao, C.-S.; Wang, B.-Z.; Shang, Y.-H. Effects of Carbopol® 934 proportion on nanoemulsion gel for topical and transdermal drug delivery: a skin permeation study. *Int. J. Nanomed.* **2016**, *11*, 5971–5987.
- (51) Zhao, H.; Wu, L.; Yan, G.; Chen, Y.; Zhou, M.; Wu, Y.; Li, Y. Inflammation and tumor progression: signaling pathways and targeted intervention. *Signal Transduction Targeted Ther.* **2021**, *6*, 263.
- (52) Dalal, P.; Rao, R.  $\beta$ -Cyclodextrin nanosponges for enhanced anti-melanoma potential of silymarin with functions of anti-oxidant, anti-inflammatory and anti-tyrosinase. *Results Chem.* **2023**, *6*, 101006.
- (53) Katiyar, S. K. Silymarin and skin cancer prevention: Anti-inflammatory, antioxidant and immunomodulatory effects (Review). *Int. J. Oncol.* **2005**, *26*, 169–176.